# On the Fluctuating Buoyancy Fluxes Simulated in a 1/10° OGCM

HONGMEI LI AND JIN-SONG VON STORCH

*Max Planck Institute for Meteorology, Hamburg, Germany*

(Manuscript received 2 May 2012, in final form 6 February 2013)

ABSTRACT

Subgrid-scale fluctuations with zero means have generally been neglected in ocean modeling, despite their potential role in affecting the oceanic state following Hasselmann's seminal paper on stochastic climate models and series of studies conducted thereafter. When representing effects of these fluctuations in a stochastic parameterization, knowledge of basic properties of these fluctuations is essential. Here, the authors quantify these properties using hourly output of a simulation performed with a global 1/10° OGCM. This study found that fluctuating buoyancy fluxes are strong in the sense that their strengths are up to one order of magnitude larger than the magnitudes of the respective mean eddy fluxes and that the fluctuations originate not only from mesoscale eddies and tropical instability waves but also from near-inertial waves, especially in the low- and midlatitude oceans. It is this wave contribution that makes the basic properties of fluctuations distinctly different from those expected from mesoscale eddies. The geographical distribution of fluctuation intensity differs from that of mesoscale eddy activity and is strongest in the low- and midlatitude oceans complemented by additional and secondary maxima in the Gulf Stream, the Kuroshio, and the Southern Ocean. The seasonality in most of the low- and midlatitude oceans, characterized by stronger fluctuations in winter than in summer, is just the opposite of that of mesoscale eddies. In the tropical oceans, the correlation length scales reach 500 km in the zonal direction but only about 30–40 km in the meridional direction, reflecting near-inertial waves with nearly zonally oriented wavecrests. Overall, these results provide an important basis for stochastically describing the effects of subgrid-scale fluctuations.

## 1. Introduction

The effects of processes not resolved in a climate model can generally be decomposed into a mean part and a fluctuating part, defined as deviations from the respective mean. The fluctuating part, even though having zero mean, can play an important role in generating large-scale low-frequency variations and in shaping mean circulations. Hasselmann and his colleagues (Hasselmann 1976; Frankignoul and Hasselmann 1977; Lemke 1977) postulated and demonstrated the role of small-scale short-term fluctuations in exciting variations of slow climate components. Watermann and Jayne (2012) showed that localized transient forcing can be crucial in generating large-scale circulations such as time-mean recirculation gyres. Beena and von Storch (2009) showed that the fluctuations in surface fluxes can, because of the nonlinearity within the system, affect the mean oceanic circulation. Palmer (2001) suggested that some of the remaining errors in weather and climate prediction models may have their origin in the neglect of subgrid-scale variability. By including small-scale fluctuations into an atmospheric GCM, von Storch (2004) found that the variability generated by unresolved processes can significantly affect the statistical dissipations of large-scale atmospheric variables. The latter can alter the climate sensitivity to external forcings (i.e., greenhouse gas concentration) and the long-term climate prediction (Seiffert and von Storch 2008, 2010). One way to take subgrid-scale fluctuations into account is to develop stochastic parameterization schemes, in which fluctuations are represented by stochastic forcings.

Various stochastic parameterization schemes have been developed, mostly designed to present the unresolved fluctuations in the atmosphere (Lin and Neelin 2000; Beena and von Storch 2009; Fraedrich 2005; Seiffert et al. 2006). With respect to unresolved fluctuations in the ocean, the role of mesoscale eddies on large-scale currents was studied by Berloff (2005) by introducing random forcing into an eddy-resolving midlatitude double-gyre ocean model. He suggested that the random forcing can potentially replace the diffusion, which is

*Corresponding author address:* Hongmei Li, Max Planck Institute for Meteorology, Bundesstrasse 53, 20146 Hamburg, Germany.
E-mail: hongmei.li@zmaw.de

DOI: 10.1175/JPO-D-12-080.1

commonly used to parameterize eddy effects on the large-scale currents. By using an idealized coupled ocean–atmosphere model of midlatitude climate, Berloff et al. (2007) further suggested that the main effects of the eddies are an enhancement of the oceanic eastward jet separating the subpolar and subtropical gyres and a weakening of the gyres; and the flow-enhancing effect is because of nonlinear rectification driven by fluctuations of the eddy forcing. As most of the state-of-the-art OGCMs do not resolve mesoscale eddies and other small-scale features, one would expect to see more studies that use stochastic parameterization to describe unresolved fluctuations in an OGCM. Ideally, these studies should take not only fluctuations resulting from mesoscale eddies but also all unresolved processes into account. To our knowledge, there exists no stochastic parameterization that is designed to represent subgrid-scale fluctuations in an OGCM under a realistic setting. This situation is directly related to the lack of knowledge about unresolved fluctuations, caused by poor temporal and spatial coverage in the observations and by the limited ability in performing global high-resolution simulations. In particular, the basic properties of subgrid-scale fluctuations, for instance the variances of these fluctuations, a crucial parameter needed to quantify the stochastic forcing in a stochastic parameterization, are essentially unknown.

The purpose of this study is to quantify the basic features of fluctuations that are simulated by an OGCM at $^1/_{10}^\circ$ resolution but likely not represented by a standard noneddy-resolving OGCM used for climate purposes, and to understand processes responsible for these fluctuations. This is the first step toward a stochastic parameterization of subgrid-scale fluctuations and a further quantification of stochastic effects of small-scale processes on general oceanic states. For this purpose, the STORM/National Centers for Environmental Prediction (NCEP) simulation (von Storch et al. 2012a,b) obtained with the Max Planck Institute Ocean Model (MPI-OM) is analyzed. The STORM/NCEP simulation together with a number of simulations obtained from regional and global eddy-resolving models (Beckmann et al. 1994; Smith et al. 2000; McClean et al. 2002; Masumoto et al. 2004; Maltrud and McLean 2005) has proved to realistically produce many features of the oceanic general circulation, including the mesoscale eddies. We will focus on fluctuations originating from small-scale short-term processes which are likely not resolved by a noneddy-resolving OGCM, even though a clear separation of processes simulated by an eddy-resolving model from those simulated by a noneddy-resolving model is difficult to achieve. To quantify fluctuations that are likely not resolved by a noneddy-resolving model, we concentrate on the high-frequency (i.e., once per hour) STORM/NCEP output to capture as much small-scale short-term variation as possible. After a description of the model, experiments, and methods in section 2, the total variances of short-term fluctuations in the STORM/NCEP simulation, which would determine the variances of stochastic forcings in a stochastic parameterization scheme, are analyzed in section 3, followed by an investigation of the seasonality of these variances in section 4 and spatial and temporal characteristics in section 5. To explore possible mechanisms responsible for the short-term fluctuations described in sections 3–5, and furthermore to quantify the extent to which the short-term fluctuations simulated by the $^1/_{10}^\circ$ simulation can also be simulated by a noneddy-resolving model, results derived from additional simulations at coarser resolutions and daily-averaged output of the STORM/NCEP simulations are discussed in section 6. Concluding remarks are given in section 7.

## 2. Model, experiments, and methods

### *a. Model and experiments*

The model used is the tripolar version of MPI-OM developed for the German consortium STORM project aimed at high-resolution climate change simulations. The model, denoted by TP6ML80 (TP = tripolar, 6M = 6 min, L80 = 80 unevenly spaced vertical levels), has a horizontal resolution of $^1/_{10}^\circ$ (i.e., about 10 km in the equatorial regions and down to a few kilometers in the Southern Ocean) and a time step of 600 s. Most of the model formulations and parameterization are the same as described by Jungclaus et al. (2006). In this high-resolution model simulation, the Gent-McWilliams (GM) parameterization (Gent et al. 1995) for mesoscale eddies is switched off.

The model is spun up for 25 years using the German ocean model intercomparison project (OMIP) atmospheric forcing (Röke 2001) based on the 15-yr European Centre for Medium-Range Weather Forecasts (ECMWF) Re-Analysis (ERA-15) (Gibson et al. 1997). After a 25-year spin up phase, the kinetic energy in the deep ocean reached a quasi-stationary state. The model is then forced by a 6-hourly atmospheric forcing derived from NCEP–National Center for Atmospheric Research (NCAR) reanalysis (Kalnay et al. 1996) for the period from 1948 to 2010. The 6-hourly atmospheric forcings are linearly interpolated to each model time step and are implemented in the ocean model thereafter. It is certainly desirable to force the ocean at a frequency higher than once every 6 h. However, higher-frequency reanalyses are not available over long time period. One should keep

TABLE 1. Experiments performed with the MPI-OM using Levitus et al. (1998) salinity and temperature as initial condition. All experiments consist of a 25-yr spin up phase, followed by a simulation driven by the surface forcing derived from NCEP–NCAR reanalysis for the period from 1948 to 2010. The middle column indicates whether GM parameterization is applied.

| | Resolution | | | | |
|---|---|---|---|---|---|
| Simulation | Lat and lon | Levels | GM | Wind forcing | Data considered |
| STORM/NCEP | ~0.1° | 80 | No | 6 hourly | Hourly and daily |
| TP10L40 | ~0.1° | 40 | Yes | 6 hourly | Hourly |
| TP04L40 | ~0.4° | 40 | Yes | 6 hourly | Hourly |
| TP04L40_smth | ~0.4° | 40 | Yes | 10-day smoothed | Hourly |

in mind that the use of 6-hourly forcing may underestimate fluctuations. We use the NCEP–NCAR wind stresses directly, which are independent of the oceanic state. These wind stresses differ from those obtained by taking ocean currents into account, as do the variations generated by the two different wind stresses. More details about the STORM/NCEP simulation can be found in von Storch et al. (2012a,b). The model was integrated for more than 80 years, that is, 25 years of the OMIP forcing run plus 63 years (1948–2010) of the NCEP–NCAR forcing run. Such long simulations are sufficient to reach quasi-equilibrium mesoscale processes. Although we use fine vertical resolution, part of the near-inertial energy in the ocean is probably associated with very small vertical scales, and this will be not well resolved by the model. We do not consider tides because the present formulation of MPI-OM does not include tides.

Apart from the STORM/NCEP run, we performed three additional experiments with MPI-OM following the same basic setup of the STORM/NCEP simulation (i.e., daily OMIP forcing over 25 years and then surface forcing derived from the 6-hourly NCEP–NCAR reanalysis). The experiments are used to assess 1) the extent to which short-term fluctuations found in the $^1/_{10}$° STORM/NCEP run can also be simulated using coarser-resolution models and 2) the dominance of processes behind the fluctuations. Even though mesoscale eddies are expected to be relevant for both issues, their precise significance with respect to fluctuating fluxes is not known. To address the first issue, two simulations using MPI-OM at a horizontal resolution of 0.4° (experiment TP04L40) and 1.0° (experiment TP10L40) using 40 vertical levels were carried out. To address the second issue, the simulation with MPI-OM at 0.4° resolution is repeated, in which the 6-hourly wind forcing is replaced by a running-averaged wind forcing with the average window being 10 days (experiment TP04L40_smth). The use of smoothed wind forcing aims at quantifying the contribution of near-inertial waves to the total fluctuations. In all three experiments, isopycnal tracer mixing by unresolved eddies is parameterized following Gent et al. (1995). A list of the experiments is given in Table 1.

### b. Methods

When concentrating on larger scales, Reynolds-averaged equations are considered. For tracer $B$, this equation takes the form of

$$\frac{\partial \overline{B}}{\partial t} + \nabla \cdot \overline{\mathbf{F}} = \overline{Q}, \tag{1}$$

where $Q$ indicates the source and sink of $B$, $F = \mathbf{V}B$ is the flux of $B$, where $\mathbf{V}$ is the velocity vector. The overbar denotes an average over unresolved temporal and spatial scales in general and a time mean (to be further specified below) in the present study. Here, $\overline{\mathbf{F}}$ is obtained by applying $\overline{(\cdot)}$ on flux $\mathbf{F}$ and represents the mean part of flux $\mathbf{F}$. The fluctuating part of $\mathbf{F}$ is defined by

$$\mathbf{F}' = \mathbf{F} - \overline{\mathbf{F}} = \mathbf{V}B - \overline{\mathbf{V}B} = (\mathbf{V}B)', \tag{2}$$

where the prime denotes deviations from the respective mean value. By definition, $\mathbf{F}'$ varies on all scales over which the average operator $\overline{(\cdot)}$ is applied.

It is noted that $(\mathbf{V}B)'$ differs from $\mathbf{V}'B' = (\mathbf{V} - \overline{\mathbf{V}})(B - \overline{B})$. $\mathbf{V}'B'$ generally has a nonzero mean and this mean represents an important component of $\overline{\mathbf{F}} = \overline{\mathbf{V}B} + \overline{\mathbf{V}'B'}$. On the contrary, the mean of $(\mathbf{V}B)'$ vanishes by definition, a feature that makes the role of $(\mathbf{V}B)'$ less obvious. As a result, $\mathbf{V}'B'$ (both its mean and its variability) has been studied by many authors using both observations and model data (e.g., Wunsch 1999; Roemmich and Gilson 2001; Jayne and Marotzke 2002; Meijers et al. 2007; Smith et al. 2000). Many efforts are made to parameterize the effects of $\overline{\mathbf{V}'B'}$ (Gent et al. 1995; Eden and Greatbatch 2008). On the contrary, $(\mathbf{V}B)'$ is generally ignored. To distinguish these two different time-varying fluxes, $(\mathbf{V}B)'$ will be referred to as the fluctuating flux and $\mathbf{V}'B'$ as the eddy flux (and accordingly $\overline{\mathbf{V}'B'}$ as the mean eddy flux). In this paper, we will concentrate on fluctuating fluxes in buoyancy, $(\mathbf{V}T)'$ with $T$ being the potential temperature and $(\mathbf{V}S)'$ with $S$ being salinity.

Consider now the exact definition of the average operator $\overline{(\cdot)}$ used in this paper. Given the form of Eq. (1),

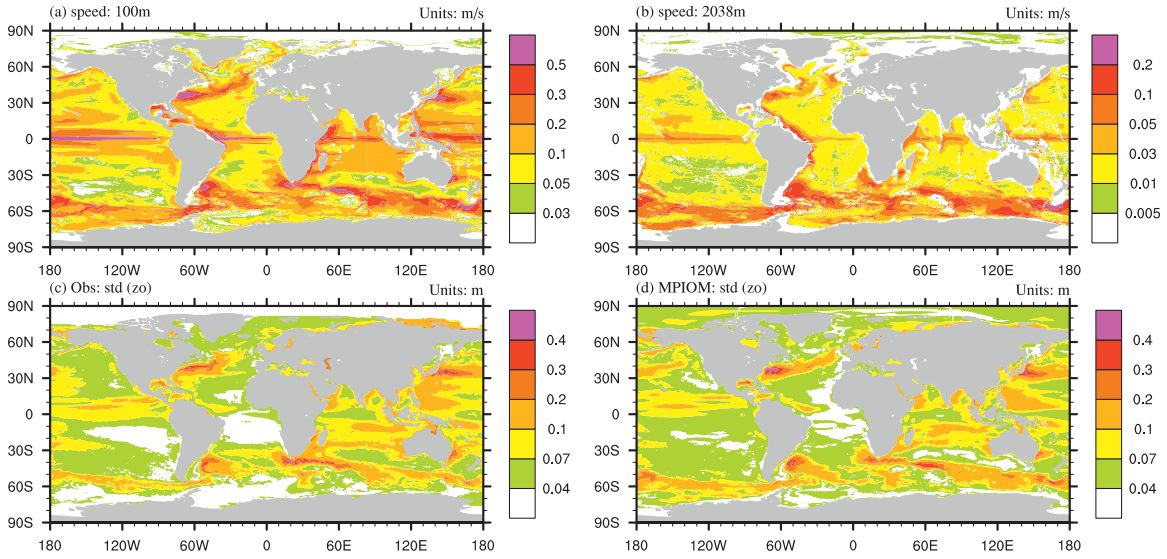


FIG. 1. Mean velocity speed ($m\,s^{-1}$) at (a) 100 m and (b) 2038 m, and (d) std dev of sea surface height (m) derived from daily output of the STORM/NCEP simulation for the period from 1991 to 2010. (c) Std dev of sea surface height (m) derived from merging the TOPEX/Poseidon and *ERS-1/-2* weekly measurements.

we expect that dynamics of $B$ will be directly affected by the divergence of fluctuations (i.e., $\mathbf{V} \cdot \mathbf{F}'$, also referred to as fluctuation divergence). For this reason, we will concentrate on $\mathbf{V} \cdot \mathbf{F}'$, rather than on $\mathbf{F}'$. When considering fluctuation divergence, an average in space becomes irrelevant, since divergence of any spatially averaged quantity vanishes. Throughout this paper, the average operator [i.e., the overbar in Eq. (2)] refers to an average over time only. This average should be designed such that the resulting fluctuations stem from as many short-term unresolved processes as possible, and at the same time, not from too many long-term resolvable processes, since the aim of the present paper is to quantify fluctuations that are not resolved by a coarse-resolution model. A part of long-term variations can, at least in principle, be simulated by a coarse-resolution model (e.g., some large-scale Rossby waves). Given that the shortest time scale available from the STORM/NCEP simulation is one hour and that one important source of the unsolved fluctuations originates from mesoscale eddies, which vary on time scales ranging from days to a few months, the primary average operator is defined as the time average of hourly data over three months. The resulting fluctuating fluxes vary on time scales ranging from one hour to three months.

Although it is not our purpose to identify the best average operator for designing a stochastic parameterization to be implemented in a GCM at a particular resolution, fluctuating fluxes obtained using different average operators are also considered to disentangle processes behind the fluctuations. The dependence of the strength of fluctuating fluxes on the average operator used will be studied.

In practice, using hourly data is subjected to some limitations. Because of the shortage in storage capacity, hourly data are stored for six months only, namely for January–March (JFM) and July–September (JAS) of 2005. The fluctuating fluxes (i.e., $\mathbf{F}'$) analyzed below are derived from hourly data in JFM 2005 by removing $\overline{\mathbf{F}}$ averaged over JFM 2005. To assess the seasonality in variations of $\mathbf{F}'$, hourly fluctuations in JAS 2005 obtained by removing $\overline{\mathbf{F}}$ for JAS 2005 are also considered. We are aware that the results derived from hourly data over one single 3-month period can suffer from sampling variability. To get a rough idea about the robustness of statistics derived from a particular year, daily data that are available throughout the STORM/NCEP simulation are considered. We calculated statistics for daily fluctuating fluxes in 20 JASs and in 20 JFMs for the period from 1991 to 2010, and compared the statistics (e.g., variance and seasonality, the latter in terms of JFM to JAS difference) in a particular year with those averaged over 20 years. The result suggests that, at least when fluctuations varying on time scales ranging from one day to three months are concerned, the gross features found for a particular year are comparable to those found in the 20-yr average.

To give the reader some idea about the mean state and mesoscale variability from STORM/NCEP simulation, mean horizontal velocity speed at 100 and 2038 m and standard deviation of sea surface height during 1991–2010 of STORM/NCEP daily output are shown in Fig. 1.

For comparison, the standard deviation of sea surface height from datasets merging the Ocean Topography Experiment (TOPEX)/Poseidon and *European Remote Sensing Satellite-1/-2* (*ERS-1/-2*) weekly measurements on a 1/3° Mercator grid are also shown in Fig. 1 (Traon et al. 1998). In the upper ocean, strong currents reside in the tropics, midlatitudes in the Northern Hemisphere, and the Antarctic. The mean velocities reflect the large-scale circulation, including the equatorial current system, the Gulf Stream, the Kuroshio, and the Antarctic Circumpolar Current (ACC). In the deep ocean, the ACC and western boundary currents dominate. The standard deviation of daily sea surface height (Fig. 1d), which provides a rough measure of mesoscale activities, shows large variations in typical mesoscale eddy active regions, that is, the Gulf Stream, the Kuroshio, and the ACC, which is consistent with observations (Fig. 1) and corresponding literature (Stammer 1997, 1998) and eddy-resolving OGCM simulations (Masumoto et al. 2004; Maltrud and McLean 2005). A comparison with Fig. 1a suggests that mesoscale eddies are active in (and are inherent to) strong current regions. More information about the STORM simulation concerning the Lorenz energy cycle and the eddying second-moment state can be found in von Storch et al. (2012a) and von Storch et al. (2012b, manuscript submitted to *J. Adv. Model. Earth Syst.*)

## 3. Total variances: Their geographical distribution and typical magnitude

In a stochastic parameterization designed to represent the effect of unresolved fluctuations, an important parameter is the variance of the stochastic forcing. This variance should be closely related to the variances of fluctuation divergence [i.e., variances of $\nabla \cdot (\mathbf{V}B)'$], which will be considered in this section. To further appreciate the strength of the variability found, we compare the standard deviation of fluctuation divergence in temperature [i.e., standard deviation of $\nabla \cdot (\mathbf{V}T)'$] with the magnitude of the better known mean eddy temperature flux divergence $\nabla \cdot \overline{\mathbf{V}'T'}$. To this end, it is noted that the zonally integrated mean meridional eddy heat flux obtained from the STORM/NCEP simulation is comparable to many previous estimates. For instance, the zonally integrated eddy heat flux obtained from the STORM/NCEP simulation reveals essentially the same structure, though somewhat stronger magnitude, as that obtained from a 1/4° OGCM simulation reported by Jayne and Marotzke (2002) (not shown).

Figure 2a shows the result for the temperature flux at 100-m depth. The variability of fluctuation divergence, as measured by the standard deviation of $\nabla \cdot (\mathbf{V}B)'$, is stronger than $1.0 \times 10^{-5}\,^{\circ}\mathrm{C\,s^{-1}}$ in most of the regions from 30°S to 40°N and has the largest values in the equatorial western Atlantic, western Indian Ocean, and western and central equatorial Pacific. There are also large values in regions of strong currents, such as the Gulf Stream, the Kuroshio, and the ACC. However, the fluctuations there are somewhat smaller than those in the tropical and subtropical oceans. This is particularly true for fluctuations in the ACC. Relative to the magnitude of divergence of the mean eddy temperature flux (i.e., $\nabla \cdot \overline{\mathbf{V}'T'}$), the strength of divergence of fluctuating temperature fluxes is about one order of magnitude larger in most of the tropical and subtropical oceans, and factors from 2 to 5 and occasionally up to 10 larger in the Gulf Stream, the Kuroshio, and the ACC.

Relative to those in the upper ocean, fluctuations are much weaker in the deep ocean. Standard deviations of fluctuation divergence in temperature at 2038 m (Fig. 2b) are from one to two orders of magnitude smaller than those at 100 m. Regarding spatial distribution, variations of fluctuation divergence in temperature are large in the tropical oceans, most of the Atlantic and Indian Ocean, and in the ACC, with the latter standing out more clearly than the corresponding values in the upper Southern Oceans. The magnitude of fluctuation divergence is more than 10 times larger than the magnitude of divergence of mean eddy flux in the tropical oceans, whereas the two are comparable in the ACC. The strong fluctuations in the deep ACC is consistent with the strong eddy kinetic energy in the deep ACC shown in von Storch et al. (2012a).

Consider now the fluctuating fluxes in salinity. The spatial distribution of the variability of divergence of these fluxes (Figs. 3a,b) bears strong similarity to that of fluctuating fluxes in temperature (Fig. 2). At 100 m, strong variations are found in most of the regions from 30°S to 40°N (Fig. 3a), as for the fluctuating temperature fluxes (Fig. 2a). Furthermore, there are also large values in regions of strong currents, such as the Gulf Stream, the Kuroshio, and the ACC, with the values in ACC being somewhat smaller. Relative to the variability of fluctuation divergence in salinity at 100 m, the variability at 2038 m (Fig. 3b) is about one order of magnitude weaker and has essentially the same spatial distribution as the corresponding flux in temperature. Relative to the magnitude of the divergence of the mean eddy salinity flux, the strength of fluctuation divergence in salinity is about one, occasionally even more than one, order of magnitude larger (not shown).

The similarity between fluctuating fluxes in temperature and salinity is related to the fact that the two fluctuating fluxes are highly correlated (Fig. 3c). The amplitude of the correlations is larger than 0.9 almost everywhere. The correlation is positive in the region extending from

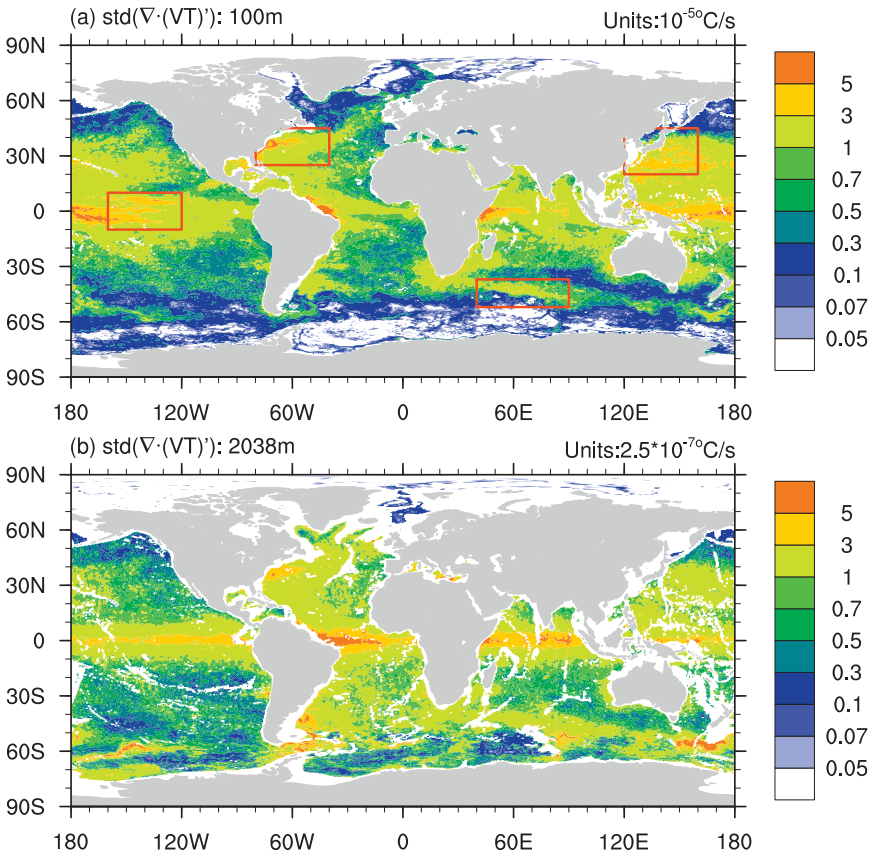


FIG. 2. Std dev of divergence of fluctuating temperature fluxes at (a) 100 m ($10^{-5}$ °C $s^{-1}$) and (b) 2038 m ($2.5 \times 10^{-7}$ °C $s^{-1}$) from STORM/NCEP simulation, derived from hourly data for JFM 2005. Red rectangular boxes show four subregions, that is, the Gulf Stream, the Kuroshio, the central tropical Pacific, and a part of the ACC, used for later statistical analyses.

60°S to 60°N, and negative east of the Antarctic Peninsula and in the Arctic. Negative correlations are also found in some coastal regions. The high correlation is caused by the fact that both $\mathbf{V}T$ and $\mathbf{V}S$ represent, in most part of the ocean away from coastal regions, products of a strongly varying variable (i.e., velocity) with a more inert quantity (i.e., $T$ or $S$) so that variations in $\mathbf{V}T$ and $\mathbf{V}S$, or equivalently variations in $(\mathbf{V}T)'$ and $(\mathbf{V}S)'$, stem essentially from those of the strongly varying variable. In the polar regions, in particular to the east of the Antarctic Peninsula and in the Arctic, temperature often drops below zero. There $T$ and $S$ have opposite signs. Correlations between $\mathbf{V}T$ and $\mathbf{V}S$ are negative. The high correlation induced by the common factor $\mathbf{V}$ is further explored in the appendix. Because of this extremely high correlation, fluctuation divergence in salinity has many features in common with fluctuation divergence in temperature. Hereafter, we will concentrate on the fluctuating temperature fluxes only.

Before continuing our analysis on fluctuating fluxes, we want to know how much of the variability in the fluctuating fluxes, as described by Fig. 2 and Fig. 3, can be simulated by a coarser-resolution model. Obviously, a model at $^1/_{10}°$ resolution can resolve much more mesoscale eddies than the same model at a lower resolution. However, as is evident from Fig. 2 and Fig. 3, strong variations in fluctuating fluxes are not exclusively confined to the expected regions of strong mesoscale eddies. In particular, large variations of fluctuating fluxes are also found in the tropical and subtropical oceans outside strong baroclinic instability.

To assess the dependence on model resolution, we performed two ocean-only experiments using MPI-OM at 0.4° and 1.0° resolution (experiments TP04L40 and TP10L40 in Table 1). Figure 4 shows the ratios of standard deviation of divergence of fluctuating temperature flux in the STORM/NCEP run to those in the TP10L40 run (Fig. 4a) and the TP04L40 run (Fig. 4b), respectively. As expected, variability in fluctuating fluxes generally decreases with decreasing resolution. The standard deviation ratios reach up to 50 for experiment TP10L40 (Fig. 4a, left) and up to 10–20 for experiment

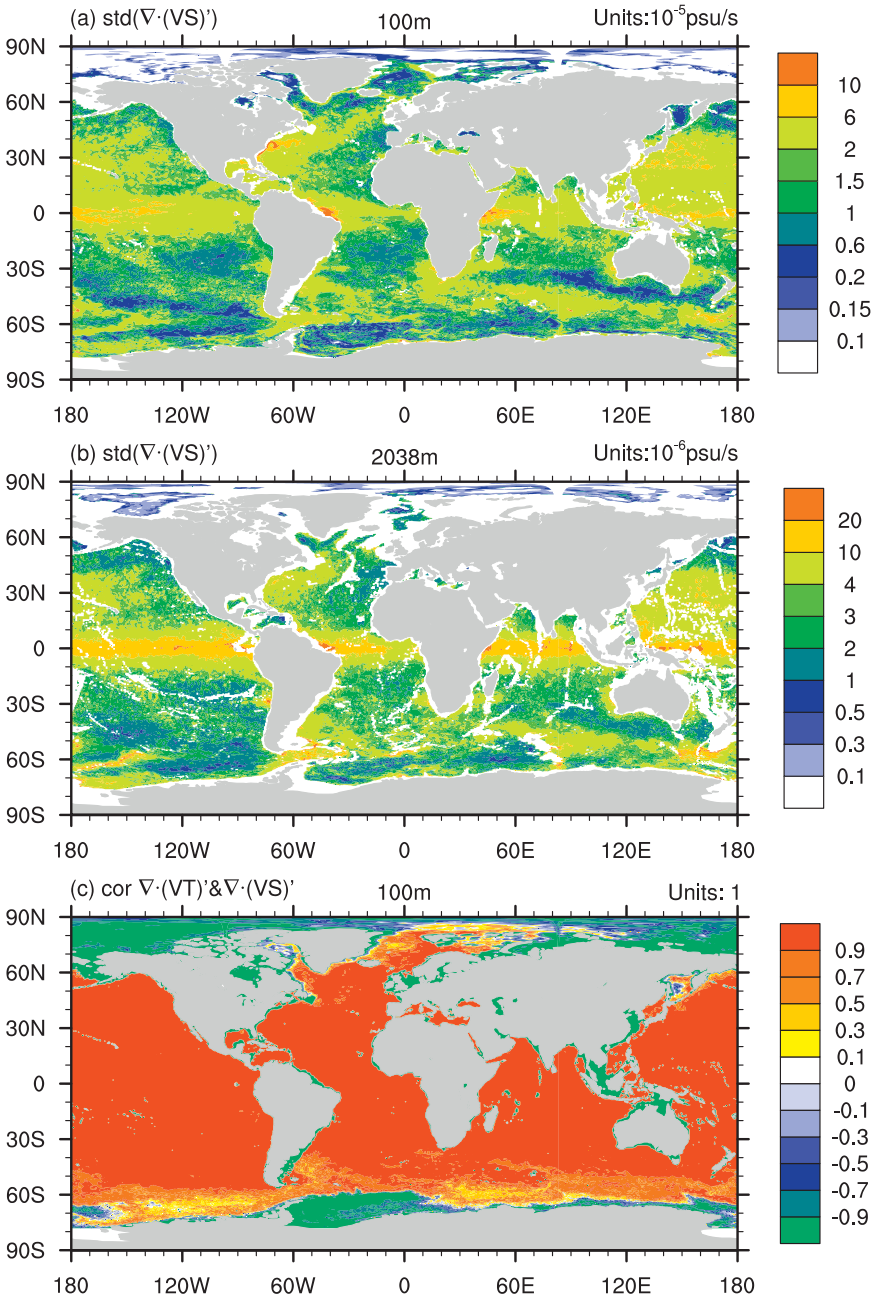


FIG. 3. Std dev of divergence of fluctuating salinity fluxes at (a) 100 m ($10^{-5}$ psu s$^{-1}$) and (b) 2038 m ($10^{-6}$ psu s$^{-1}$), and (c) correlations between divergence of fluctuating temperature and salinity fluxes at 100 m. The hourly data for JFM 2005 are used.

TP04L40 (Fig. 4b, left) in regions with strong eddy activities, for instance in the Gulf Stream and North Atlantic Current and in the ACC. The way that the resolution dependence varies with latitude is described by two different regimes, one characterized by a band of small ratios in the tropical oceans and the other by two bands of large ratios in the northern and southern subtropical and midlatitude oceans. The simulated variability is less strongly affected by the resolution in the first than in the second regime. This difference is more clearly demonstrated by the zonally averaged ratios (Fig. 4, right). When reducing resolution from 0.1° to 0.4° (Fig. 4b, right), the variability is halved near the equator in the first regime, but reduced by about 10%–15% near 30°N and 40°S in the second regime. Similarly, when reducing resolution from 0.1° to 1° (Fig. 4a, right), the variability is

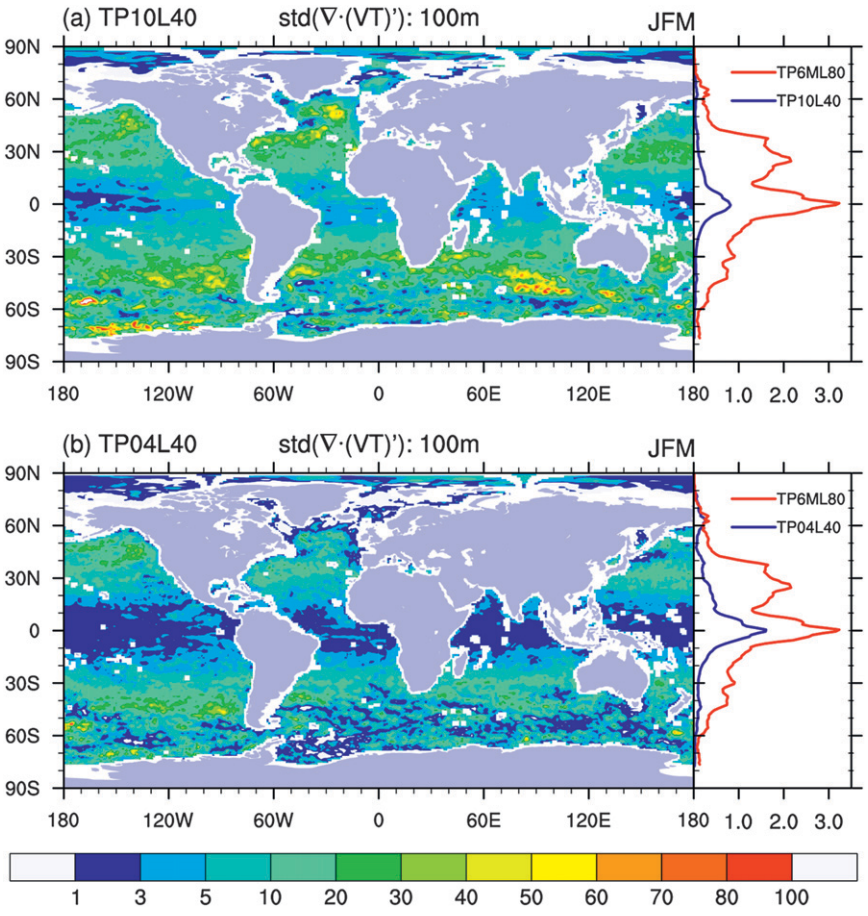


FIG. 4. Ratios of std dev of fluctuation divergence simulated by STORM/NCEP to that simulated by (a) TP10L40 and (b) TP04L40 at (left) 100 m and (right) the respective zonally averaged ratios. The hourly data for JFM 2005 are used.

reduced by about 25% near the equator, but by 6%–8% near 30°N and 40°S. This difference suggests that variations from other unresolved processes, such as wind-induced near-inertial waves or tropical instability that dominate in the tropical oceans, can be partly simulated using coarse-resolution models. In general, variations in both regimes are, to different degrees, sensitive to horizontal resolution.

## 4. Seasonality and its cause

The strength of fluctuating fluxes can vary according to seasons. We quantify this seasonality by comparing the variability in hourly fluctuations in JFM 2005 with that in JAS 2005. The results are expressed in terms of ratios of standard deviations of fluctuation divergence in JFM to those in JAS in Fig. 5 and Fig. 6. For fluctuations in both temperature and salinity, the seasonality reveals the following two features. First, in the subtropics outside the mesoscale eddy active regions, the wintertime fluctuations are much stronger than summertime ones (Figs. 5a,b), characterized by JFM-to-JAS ratios larger than one in the Northern Hemisphere and smaller than one in the Southern Hemisphere. The large wintertime-to-summertime ratios are also found at 2038-m depth (not shown), especially in the Northern Hemisphere. Second, in the core regions of strong currents, that is, in the Gulf Stream, the Kuroshio, and occasionally also in the ACC regions, the variations of the fluctuation divergence are slightly stronger in summer than in winter (Figs. 6a,b). This seasonality weakens in the deep ocean (not shown).

The first feature can originate from wind stress forcing, as the storm-track activity is also weak and shifts poleward during summertime (Hoskins et al. 1983; Trenberth 1991). Indeed, the wintertime-to-summertime ratios of wind stress variations (Fig. 5d) reveal a pattern similar to the fluctuation divergence ratios in the subtropical and midlatitude regions. According to sections 5 and 6, a large portion of fluctuations in the subtropical

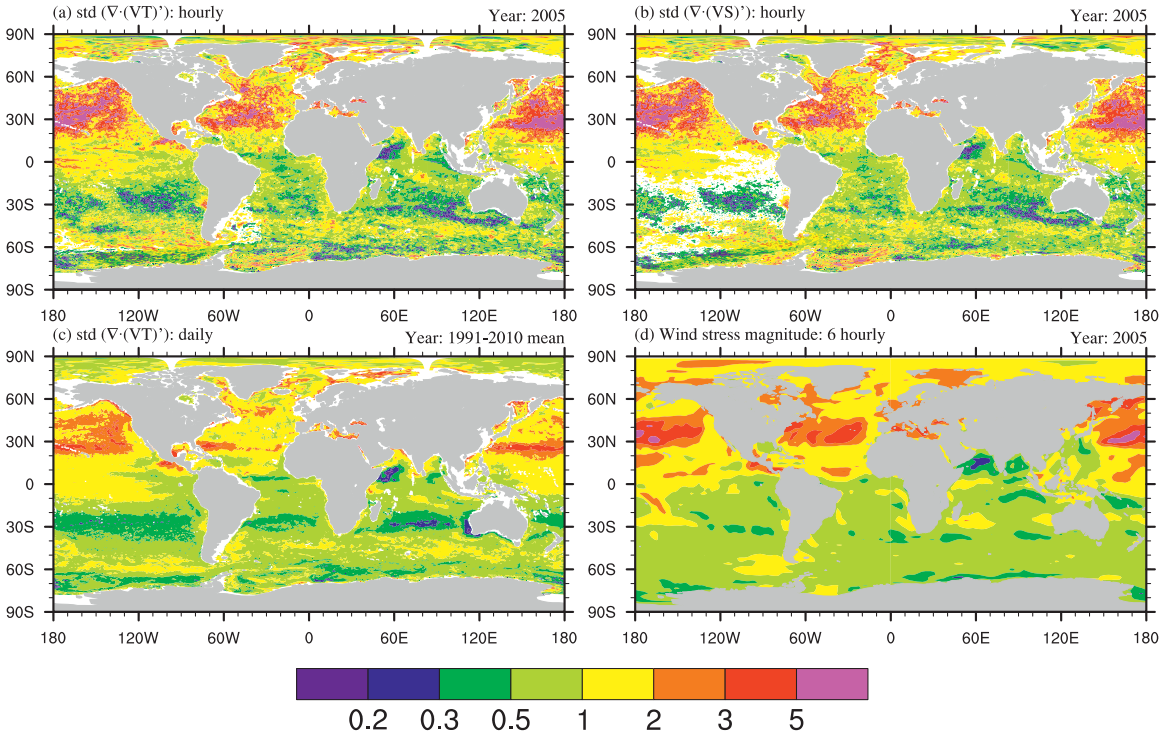


FIG. 5. Ratios of std dev of (a) fluctuating temperature and (b) salinity fluxes in JFM to those in JAS, as derived from hourly data for 2005, (c) the same ratios for temperature fluxes derived from daily data from 1991 to 2010, and (d) ratios of std dev of wind stress magnitude in JFM to those in JAS as derived from NCEP–NCAR wind forcing in 2005.

and midlatitude oceans result from near-inertial waves. Since the generation of near-inertial waves via surface winds is directly related to the strength of the winds, Fig. 5d suggests that the stronger wintertime than summertime variations are induced by the seasonality in winds.

The second feature seems to be related to seasonality in the strength of strong eddy activities as shown by JFM-to-JAS ratios of standard deviations in velocity speed in Figs. 6e,f. The mesoscale eddy activities are stronger in summer than in winter in the Gulf Stream and the Kuroshio. This seasonality is also found by other studies. Stammer et al. (2001) reported similar annual cycle in the Gulf Stream region with variability of eddy kinetic energy reaching maximum in late summer. They also found that the correlation with wind forcing increases away from strong eddy kinetic energy. By using observation and reanalysis data, Zhai et al. (2008) found that the eddy kinetic energy peaks in summer in the Gulf Stream region, which results from a reduction in dissipation in summer compared to winter.

We emphasize the difference between the seasonality discussed here and that reported by most of the previous studies. We are interested in the seasonality of fluctuations that result from as many short-term processes as possible (within the framework of the present formulation of MPI-OM that does not include tides), whereas most of the previous studies were concentrated on the seasonality related to mesoscale eddies only. The presence of wind-induced near-inertial waves leads to differences to previous studies. In particular, the seasonality characterized by stronger variations in winter than in summer in the subtropical oceans (for example 25°–35°N) opposes that obtained by focusing on mesoscale eddies only in Zhai et al. (2008; their Fig. 4c showing stronger eddy kinetic energy in summer between 15° and 35°N). Stammer et al. (2001) did not find the significant seasonality of eddy kinetic energy along the path of the North Atlantic Current and south of about 30°N in the Atlantic.

It should also be noted that the results shown in Figs. 5a,b and Figs. 6a,b are derived from a single year. To assess the robustness of these results, we calculated the same ratios from daily data for each year from 1991 to 2010. The averages of these ratios are shown in Fig. 5c and Figs. 6c,d. Using daily data will substantially reduce the contributions from near-inertial waves, in particular poleward of 30° where inertial periods are smaller than one day. As a result, the extremes in low- and midlatitude oceans in Fig. 5c are somewhat smaller than those in Fig. 5a, in particular north of 30°N in the North Atlantic and in the western and central North Pacific. The situation is more clearly demonstrated by Figs. 6c,d,

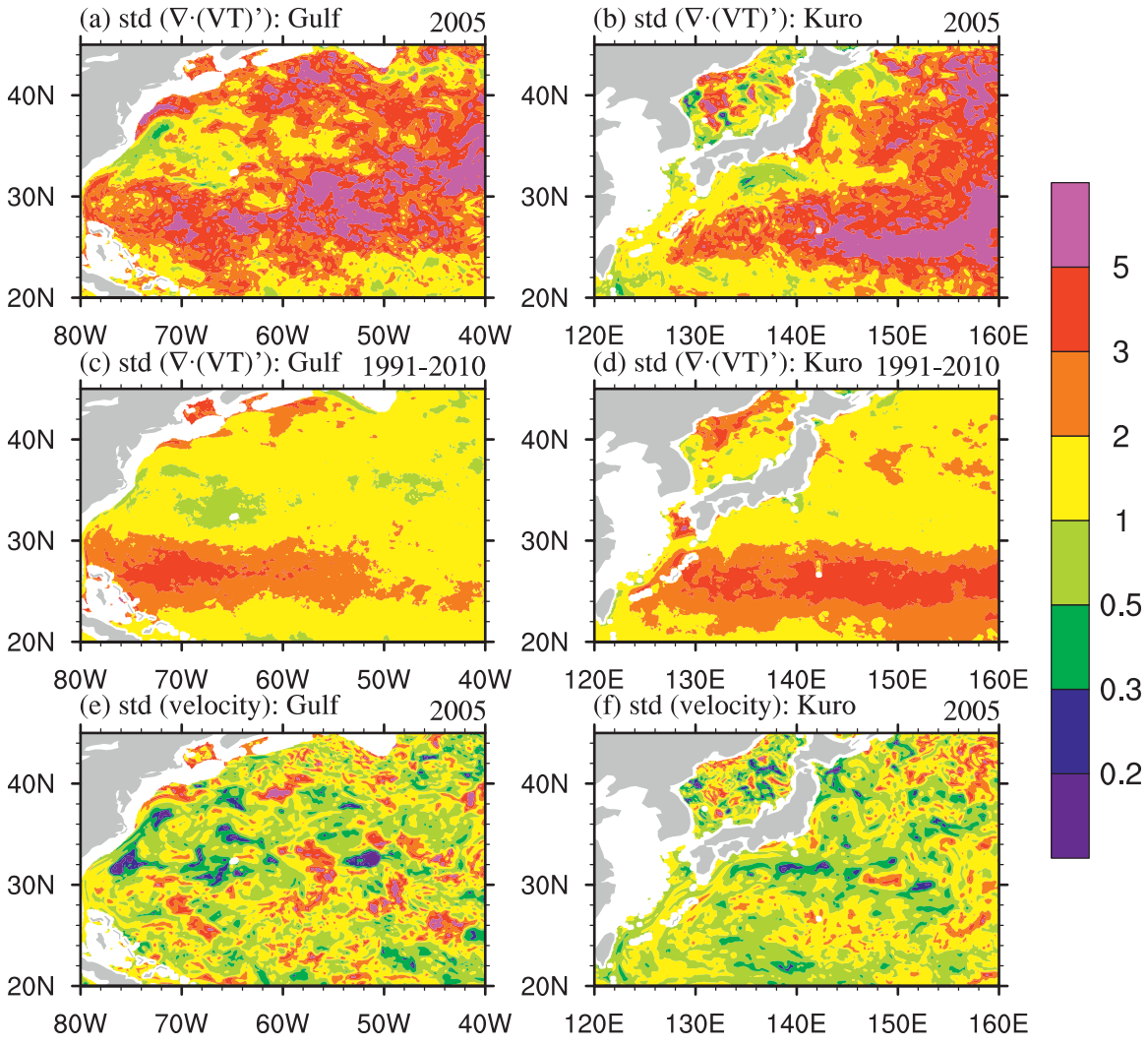


FIG. 6. Enlargements of (a),(b) Fig. 5a and (c),(d) Fig. 5c and (e),(f) std dev of velocity speed in 2005 in the (left) Gulf Stream and (right) Kuroshio regions.

showing that when using multiyear daily data, the stronger wintertime than summertime fluctuations north of 30°N are strongly reduced. The other aspect of the seasonality, namely slightly stronger summertime fluctuations in Gulf Stream and the Kuroshio, is less strongly affected by the use of daily data. However, as the location of eddies and hence the position of JFM-to-JAS ratios vary from year to year, the averaged ratio is only smaller than one in very limited regions. Nevertheless, Fig. 5c and Figs. 6c,d indicate directly or indirectly that the features derived from hourly data are robust, even though it should be further confirmed by using multiyear hourly data.

## 5. Spatial and temporal characteristics

To study spatial properties of the fluctuations, Fig. 7 shows a global map of horizontal spatial length scale based on spatial correlations used in Núñez-Riboni et al. (2005). The correlations are obtained using

$$R_{i,j}(m,n)=\frac{1}{2}\left[\frac{\sum_{t=1}^{N} f_{i,j,t}\cdot f_{i+m,j+n,t}}{\left(\sum_{t=1}^{N} f_{i,j,t}^2 \sum_{t=1}^{N} f_{i+m,j+n,t}^2\right)^{1/2}} + \frac{\sum_{t=1}^{N} f_{i,j,t}\cdot f_{i-m,j-n,t}}{\left(\sum_{t=1}^{N} f_{i,j,t}^2 \sum_{t=1}^{N} f_{i-m,j-n,t}^2\right)^{1/2}}\right], \quad (3)$$

where $i$, $j$, and $t$ indicate model zonal grid number, model meridional grid number, and temporal sample number,

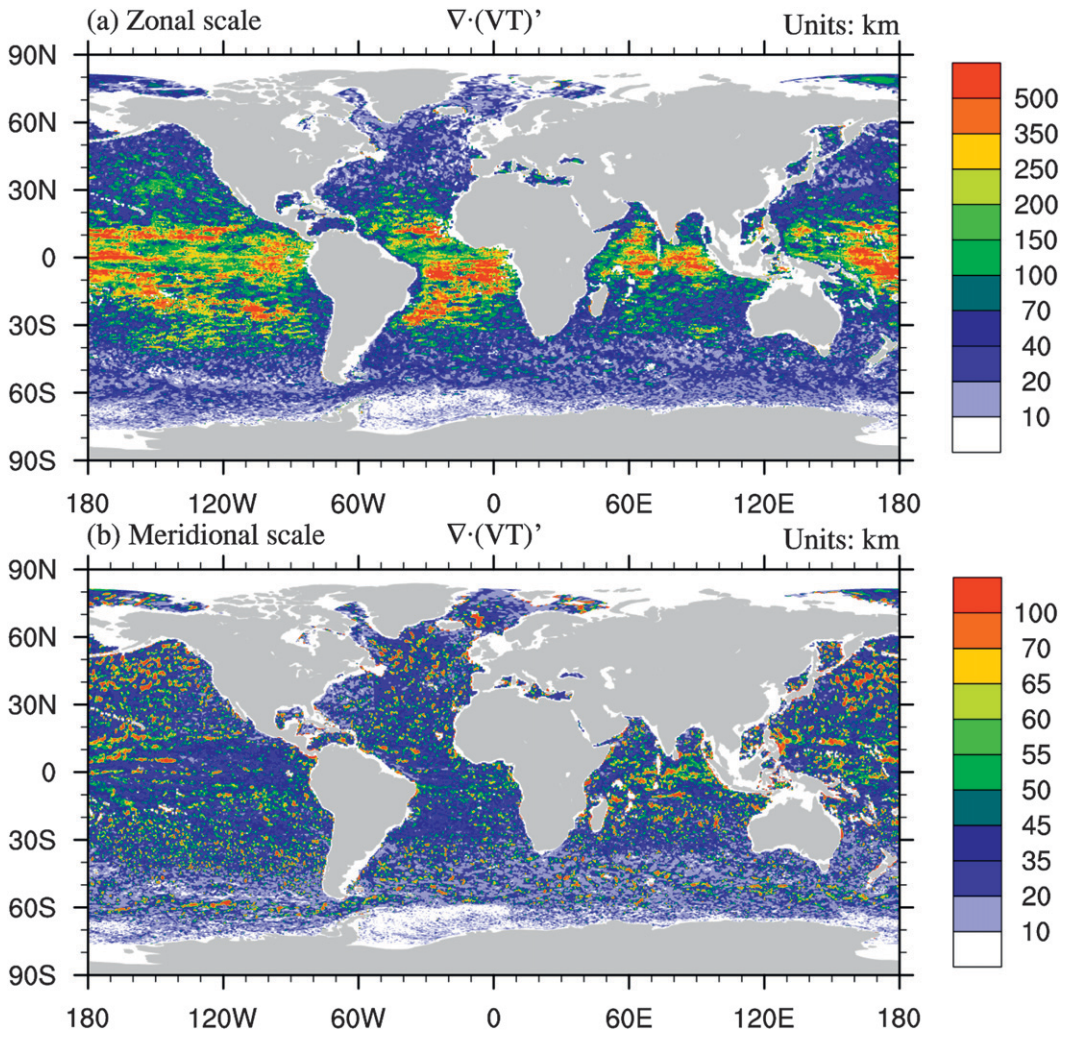


FIG. 7. Correlation scales of fluctuating temperature flux divergence at 100-m level in (a) zonal and (b) meridional direction, defined in terms of distances where the respective correlation between the reference grid and surrounding grids drops below 0.1. The hourly data for JFM 2005 are used.

respectively. Total number of temporal samples available is denoted by $N$. Hence, the correlation $R$ is a function of the number of grid cells in the zonal $m$ and meridional $n$ direction. To distinguish the scales in different directions, we calculate zonal and meridional scales separately. Using Eq. (3), the zonal scales are obtained by setting $n = 0$ and the meridional scales are obtained by setting $m = 0$. Since correlations drop with increasing $m$ and $n$, we define the zonal (meridional) scale in terms of the $m$ ($n$) at which $R$ drops below 0.1. A correlation of 0.1 is statistically significant at 0.01% level. These values of $m$ and $n$ are turned into spatial scales by multiplying them with the grid distance of about 10 km.

In the tropics, the zonal correlation scale of up to 500 km (Fig. 7a) is much larger than the meridional correlation scale of about 30–40 km (Fig. 7b). According to the discussion in section 4 and results to be shown later in this section and in section 6, part of fluctuations in low- and midlatitude oceans originate from near-inertial waves. The large difference between the zonal and meridional scales is consistent with the equatorward propagating near-inertial waves with nearly zonally oriented wavecrests. Both the equatorward propagation and the nearly zonally oriented wavecrests are distinct features in a movie composed of hourly vertical velocity anomalies. Similar wave structures are found by Komori et al. (2008) and Blaker et al. (2012). We also see these waves in movies that are made of a sequence of hourly zonal and meridional velocity anomalies. However, they are more evident outside the equatorial regions. In the equatorial oceans, horizontal velocity anomalies do not

propagate in the form of regular waves and are characterized by larger scales in the zonal than in the meridional direction (but not so dramatic as in case of near-inertial waves) and longer time scales.

In the Gulf Stream, the Kuroshio, and the ACC regions, and especially in the ACC region, the spatial correlation scales are much smaller than those in the tropics and subtropical regions. In the mid-to-high-latitude ocean, there is a general tendency of a poleward decrease in both zonal and meridional scales. The tendency is most clearly seen in the Southern Ocean, characterized by a decrease in length scales from mostly above 20 km near 40°S to between 10 and 20 km around 50°–60°S and often below 10 km south of 60°S. This tendency, which is consistent with the decrease of the first baroclinic Rossby radius with increasing latitude [see, e.g., Smith et al. (2000)], suggests the important role of mesoscale eddies in determining the characteristic length scales there.

The length scales shown in Fig. 7 reflect short-term fluctuations to a considerable extent. When repeating the same analysis for 3-day running-averaged data (not shown), both the zonal and meridional scales increase in regions of strong mesoscale eddies from around 50 to 70 km, and decrease somewhat equatorward, in particular in the region between 30° and 50°, where near-inertial variations dominate (see Fig. 10, described in greater detail below). Additional analyses are required to quantify the process that determines the spatial scales of the low-frequency variations there.

To explore temporal scales, we consider first the time series of fluctuation divergence (Fig. 8). Standard deviations of these time series (gray solid lines) are much larger than the magnitude of the divergence of the mean flux (gray dashed lines), consistent with the result of the previous section. Comparing the top with the bottom panels reveals that variations are stronger and the time scales of the variations are longer in the regions of strong currents.

To investigate the characteristic time scales, spectral analysis is performed for hourly time series in various regions. Here, we concentrate on regions indicated by the boxes in Fig. 2a. For each box, spectra of grid points in the box are averaged conditioned upon the magnitude of velocity speed. Red lines indicate the average over spectra at grid points inside strong currents and blue lines the mean spectra away from strong currents (Fig. 9). Consistent with the time series shown in Fig. 8, spectral analyses suggest that the time scales depend strongly on velocity speed. In particular, spectra in extratropical regions with strong currents reveal maxima at subinertial frequencies, whereas spectra in regions with weak currents show pronounced peak near-inertial frequency. Furthermore, the spectra in strong currents outside the tropical oceans (red lines in Figs. 9a,c,d) reveal two peaks, one at a period of 20–40 days that corresponds to the time scales of mesoscale eddies and a second one at a near-inertial period (identified by the gray bars at the upper edge of each diagram), reflecting near-inertial waves. In the tropics, major variations in strong currents are on time scales of about 20–40 days, this is consistent with the hypothesis of tropical instability waves by Jayne and Marotzke (2002). Near-inertial waves could also contribute to the spectral peak at the frequency slightly higher than 0.01 cycles per hour. However, this contribution is moderate, as the inertial frequencies at grid points considered in Fig. 9b range from $2.9 \times 10^{-3}$ to $1.4 \times 10^{-2}$ cycles per hour (gray bar near the top of Fig. 9b) and are hence mostly below the peak frequency.

## 6. Possible mechanisms responsible for fluctuations

The analyses in the previous sections reveal the characteristics of fluctuating fluxes and their possible relations to inertial waves, mesoscale eddies, and tropical instability waves. In this section, two attempts are made to further quantify possible mechanisms responsible for the fluctuations. One concentrates on midlatitude regions and the other on the tropical and subtropical regions.

At mid- and high latitudes, mesoscale eddies and near-inertial waves have distinctly different time scales. The former vary on time scales from weeks to a few months, while the latter have time scales of less than one day. By recalculating the standard deviations of fluctuating fluxes using daily data, the near-inertial wave contribution can be strongly reduced poleward of 30°. In our first attempt, the ratios of the standard deviation of fluctuations obtained from hourly data to that obtained from daily data are evaluated to assess the relative importance of mesoscale eddies and inertial waves in generating fluctuations. Poleward of 30°, where the daily average efficiently removes near-inertial oscillations, the ratios are expected to be around 1, when fluctuations are generated mainly by eddies, and much larger than 1 when they arise essentially from inertial oscillations. Figure 10 shows that the standard deviation ratios are larger than 2 in most regions between 30° and 50°, indicating the dominance of inertial oscillations there, consistent with the role of wind forcing in generating near-inertial waves discussed in section 4. Further poleward, in particular in the regions of strong mesoscale eddies in the Southern Ocean (indicated by large standard deviations of sea level in Fig. 1c, e.g., to the southeast of Argentina), the values of standard deviation ratio in Fig. 10 are between 1 and 1.5, indicating the dominance of mesoscale eddies. A further inspection

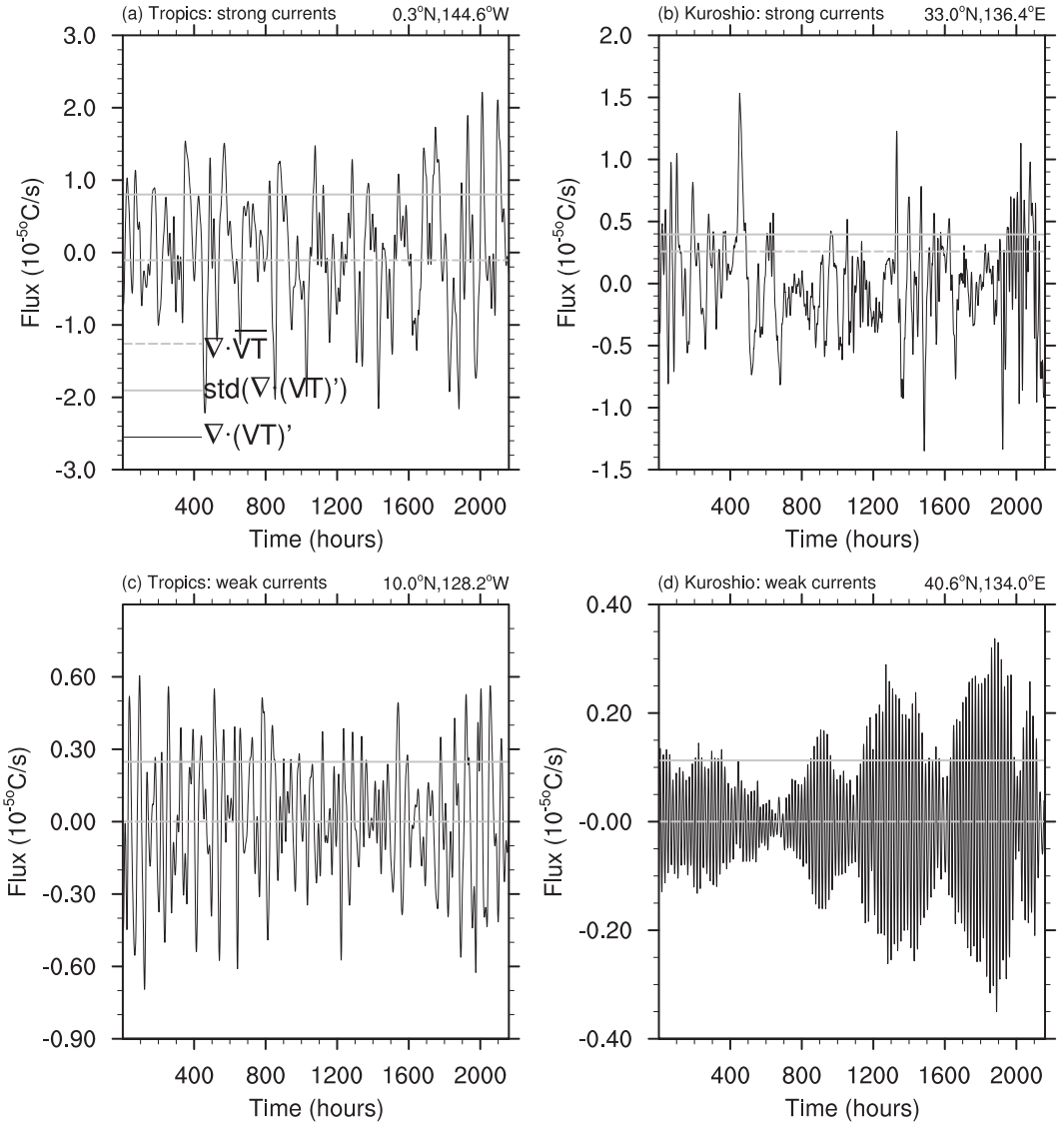


FIG. 8. Hourly time series of fluctuating temperature flux divergence ($10^{-5}$ °C s$^{-1}$; solid black curve) for JFM 2005 at representative grid points inside (a),(c) the central tropical Pacific box and (b),(d) the Kuroshio box marked in Fig. 2a. The grid points in the upper panels are located in strong current regions with maximum mean velocity speed and the grid points in the lower panels are located in weak current regions with minimum velocity speed. The respective mean eddy temperature flux divergence and std dev of fluctuating temperature divergence are shown by the dashed and solid gray lines, respectively.

reveals that more than 70% of the hourly variance south of 60°S result from mesoscale eddies.

The maximum values along 30° in Fig. 10 reflect the fact that variations on time scales shorter than 1 day arise mainly from inertial waves and that utilizing daily mean is most efficient in removing those oscillations at 30° where the inertial period is 1 day. At all other latitudes, the daily average cannot completely remove the inertial oscillations. The ratios, though still large, are smaller than those along 30°. We leave out the discussion of the ratios equatorward of about 30°, since the daily average does not lead to a clear separation between eddies and inertial oscillations there. Overall, near-inertial oscillations contribute substantially to fluctuations in most parts of the subtropical-to-midlatitude oceans.

Our second attempt aims to assess the processes behind the tropical fluctuations, in particular to quantify the role of external wind forcing versus that of internal tropical instabilities. For this purpose, we force MPI-OM with low-pass-filtered winds that strongly suppress the wind-generated inertial waves, and compare the results with the standard run forced by 6-hourly wind

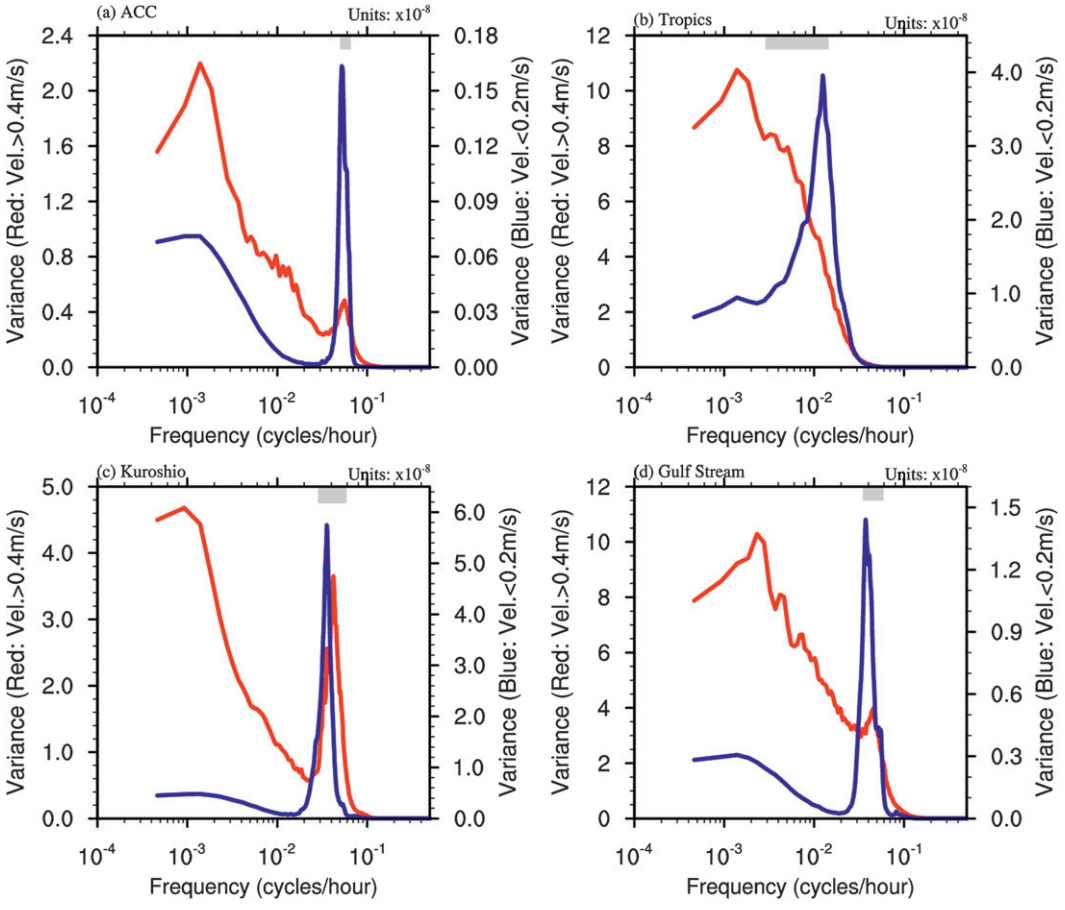


FIG. 9. Spectra of fluctuation divergence averaged over grid points inside the four boxes in Fig. 2a: (a) the ACC, (b) the tropics, (c) the Kuroshio, and (d) the Gulf Stream. Red (blue) lines represent spectra averaged over grid points with velocity speed being larger than 0.4 m $s^{-1}$ (smaller than 0.2 m $s^{-1}$). Because the period of inertial waves reaches to infinity along the equator, 2°S–2°N is excluded from the calculation of the mean spectrum in the tropical central Pacific box in (b). Hourly data for JFM 2005 are used. Ranges for inertial frequencies inside each region are indicated by horizontal gray bars.

forcing. Assuming that a notable portion of the tropical and subtropical fluctuations have large spatial scales and can be simulated using MPI-OM with 0.4° resolution, an assumption supported by Fig. 4b, we performed two experiments with MPI-OM at 0.4° resolution. One (experiment TP04L40) was driven by the same forcing as in the STORM simulation and the other (experiment TP04L40_smth) by the same forcing except that the 6-hourly wind stresses were replaced by low-pass-filtered wind stresses. We used a running average with an averaging window of 10 days. Clearly, this running average is only capable of suppressing the wind-induced inertial waves poleward of about 3°, where inertial periods are smaller than 10 days. If tropical fluctuations represent near-inertial waves generated by wind forcing, a large portion of the fluctuations in experiment TP04L40 would not be reproduced in experiment TP04L40_smth. On the other hand, if tropical fluctuations originate from tropical instabilities, a large portion of fluctuations in experiment TP04L40 would be reproduced by experiment TP04L40_smth.

Figure 11 summarizes the results of the two experiments. In most of the tropical and subtropical oceans, the standard deviation of fluctuation divergence simulated by TP04L40_smth accounts only for 10%–20% (white areas in Fig. 11) of the standard deviation simulated by TP04L40, indicating the dominance of the wind-induced inertial waves in these regions. The result is consistent with the seasonal dependence on the strength of wind stress discussed in section 4. Internal processes, such as tropical instabilities, become more prominent near the equator. For instance, they can amount to more than 70%–80% in the tropical Pacific between 8° and 3°N and between 3° and 5°S. Large variability that is not induced by winds is also found in the western tropical North Atlantic.

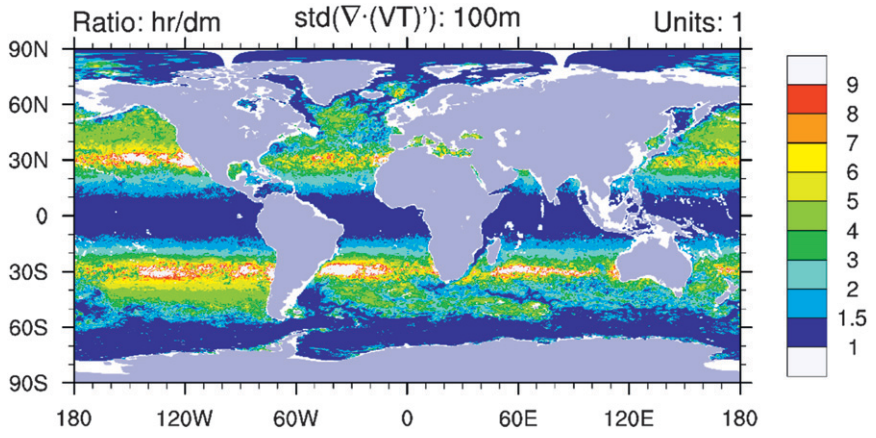


FIG. 10. Ratios of std dev of fluctuation divergence obtained from hourly data to that obtained from daily data of STORM/NCEP simulation. The data for JFM 2005 are used.

## 7. Concluding remarks

Stochastic effects of unresolved fluctuations have often been neglected in ocean modeling because their means vanish. When representing these effects in terms of a stochastic parameterization, it is essential to know the basic properties of these fluctuations, such as the geographical distributions of their variances, their seasonality, and their spatial and temporal characteristics. The variances are a crucial parameter needed to constrain the stochastic forcing in a stochastic parameterization. The other properties are necessary for further specification of the stochastic forcing. We made a first step in this direction by investigating fluctuating buoyancy fluxes using hourly output of the $^1/_{10}°$ STORM/NCEP simulation. Possible mechanisms responsible for these fluctuations and the extent to which these fluctuations can be represented using coarser-resolution simulations are further quantified by comparing the hourly output with daily output and by comparing the $^1/_{10}°$ simulation with simulations performed with MPI-OM at low and medium resolutions forced with the same surface fluxes as in the STORM/NCEP simulation and with low-pass-filtered wind forcing.

The main result of this paper is twofold. First, fluctuating buoyancy fluxes are strong in the sense that their strengths are up to one order of magnitude larger than the magnitudes of the respective mean eddy fluxes [which are the object of mesoscale eddy parameterization considered by, e.g., Gent et al. (1995)]. Second, the fluctuations originate not only from mesoscale eddies but also, at least to a considerable extent, from near-inertial

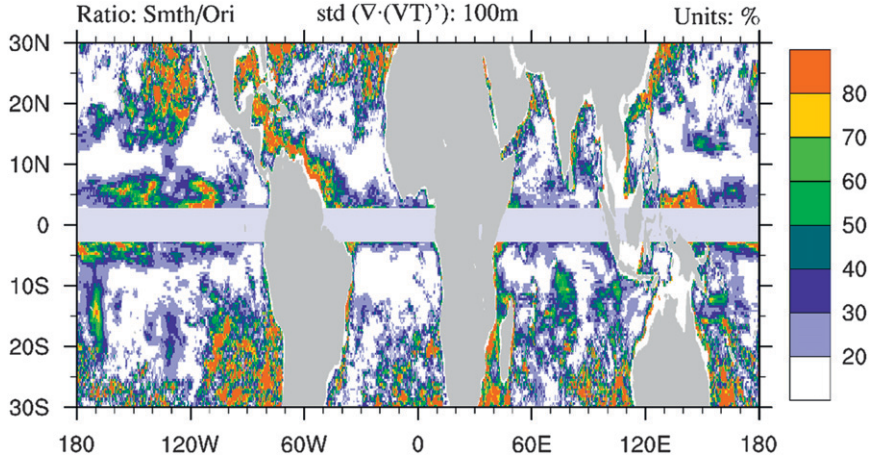


FIG. 11. Percentage of std dev of fluctuation divergence simulated by MPI-OM TP04L40 with 10-day smoothed wind forcing to that simulated by MPI-OM TP04L40 with 6-hourly wind forcing. The equatorial region from 3°S to 3°N is left out because the 10-day running average mainly excludes near-inertial waves from 3° poleward. The data for JFM 2005 are used.

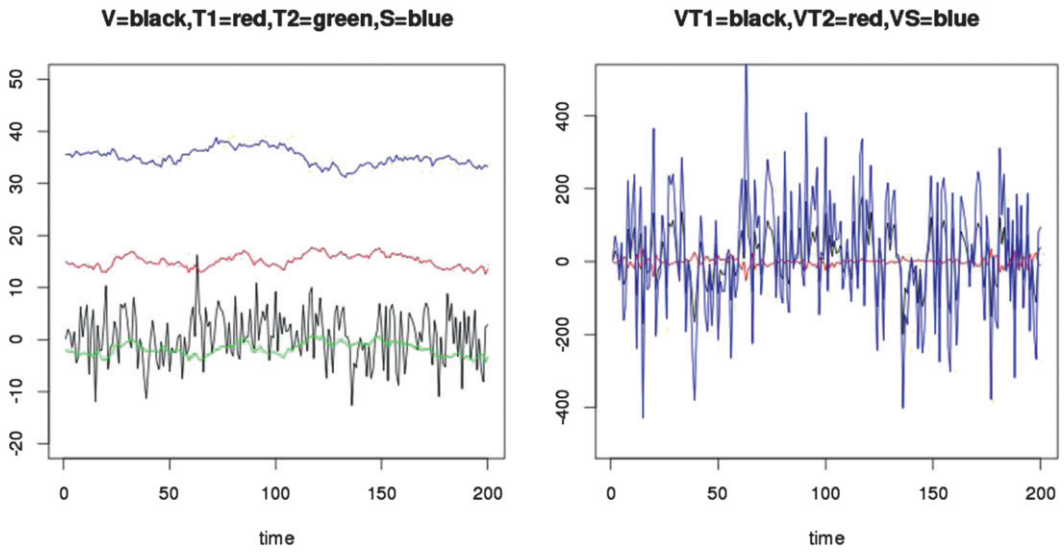


FIG. A1. (left) Time series of $V$ (black), $T_1$ (red), $T_2$ (green), and $S$ (blue) and (right) products of time series $V(T_1)$ (black), $V(S)$ (blue), and $V(T_2)$ (red).

waves, especially in the low- and midlatitude oceans. The contribution from near-inertial waves makes fluctuations in the STORM/NCEP simulation behave differently than those resulting from mesoscale eddies. The difference has the following three aspects. First, the geographical distribution of the strength of fluctuations differs from that expected from mesoscale eddies. The former is characterized by strong intensity in most of low- and midlatitude oceans (Fig. 2), complemented by additional and secondary maxima in Gulf Stream, the Kuroshio, and the ACC. The latter, on the other hand, only reveals the strong intensity in the Gulf Stream, the Kuroshio (including their extension regions), and the ACC (Fig. 1c), and has much weaker variability in most of the tropical and subtropical oceans. Second, because of the strong dependence of near-inertial waves on the wind forcing, the wintertime fluctuations are stronger than summertime fluctuations in the subtropical and midlatitude oceans outside the core regions of mesoscale eddies. This result opposes the seasonality related to mesoscale eddy activity, which is stronger in summer than in winter (Zhai et al. 2008). Finally, because of near-inertial waves with their nearly zonally oriented wavecrests, characteristic zonal scales up to 500 km are found, whereas characteristic meridional scales reach only about 30–40 km. Such a strong anisotropy is not expected by mesoscale eddies. Overall, the contribution from near-inertial waves decreases with increasing latitude. Because of high correlation between fluctuation divergence in salinity and temperature, a description of fluctuation divergence in temperature used in a parameterization of the fluctuating buoyancy fluxes can be directly transformed to a description of fluctuation divergence in salinity. One does not need to consider fluctuating salinity flux separately.

In this paper, we consider fluctuating fluxes that vary on time scales ranging from one hour to three months. Our aim is to identify the basic properties of these fluxes, rather than to quantify fluctuations not resolved by an ocean model at a particular resolution, as it is the case in Berloff (2005). Nevertheless, we did provide some estimates of the portion of the fluctuations in the $^1/_{10}°$ STORM/NCEP simulation that can be generated by the same model but at 0.4° and 1° horizontal resolution. More explicitly, the low- (1.0°; TP10L40) and medium-resolution (0.4°; TP04L40) models can produce 25% and 50% of the fluctuations found in the high-resolution (0.1°; STORM/NCEP) run near the equator, respectively (see Fig. 4). However, farther away from the equator, fluctuations are more sensitive to resolution and an increasingly large portion of fluctuations will not be simulated using coarse-resolution models.

The characteristics of fluctuations in this study provide us a basis for designing stochastic parameterization that describe the unresolved fluctuations and for further exploring the effects of these fluctuations on the general circulation. The small horizontal scales in the Gulf Stream, the Kuroshio, and the ACC regions suggest that for models with resolution larger than ~1.0°, the fluctuations in these regions can be described by spatially uncorrelated white noise. More attention should be paid to tropical fluctuations, which have larger spatial scales. As discussed in sections 3 and 6, these fluctuations result from tropical instability waves and wind-induced

near-inertial waves, which can be partially simulated using coarse-resolution OGCMs. Generally, different representations of fluctuations in and outside the tropical oceans of coarse-resolution models should be taken into account when developing a new stochastic parameterization.

*Acknowledgments.* Hongmei Li is supported by the Integrated Climate System Analysis and Prediction (CliSAP) cluster of University Hamburg. The authors are grateful to Irina Fast, Helmuth Haak, and other STORM project members for making the high-resolution model simulation available. Thanks to Helmuth Haak for his assistance in setting up low- and medium-resolution model simulations and to Ismael Núñez-Riboni and Chao Li for helpful suggestions and comments. We acknowledge Kenji Shimizu, Jochem Marotzke, and Jürgen Kröger for internal reviewing and helping us improve this paper.

## APPENDIX

### High Correlations Induced by a Strongly Varying Common Factor

High correlations between divergence of fluctuating temperature flux $V(T)$ and that of fluctuating salinity flux $V(S)$ result from the strongly varying common velocity $V$. In other words, if variations in both $V(T)$ and $V(S)$ are dominated by those of $V$, $V(T)$ would vary in the same way as $V(S)$. A high correlation between $V(T)$ and $V(S)$ will be obtained. To demonstrate this, we construct synthetic time series $V$, $T_1$, $T_2$, and $S$ using

$$\begin{aligned} V &= 5a + 0.2, \\ T_1 &= 0.5b + 15, \\ T_2 &= 0.5b - 1.9, \quad \text{and} \\ S &= 0.5c + 35, \end{aligned}$$

where $a$, $b$, $c$, and $d$ are first-order auto-regressive processes with process coefficients 0.1 for $a$, 0.98 for $b$, and 0.95 for $c$. Because of this choice of $a$, $b$, and $c$, $V$ varies on much shorter time scales than $T_1$, $T_2$, and $S$. The variability in $V$ is further strengthened by the factor 5 and the variability in $T_1$, $T_2$, and $S$ is further weakened by the factor 0.5. The offsets 0.2, 15, −1.9, and 35 crudely simulate the mean values of velocity, temperatures in the subtropical and polar regions, and salinity, respectively. The time series of $V$, $T_1$, $T_2$, and $S$, and the products $V(T_1)$, $V(T_2)$, and $V(S)$ are shown in Fig. A1. By construction, variations in $V$ dominate those in $V(T_1)$, $V(T_2)$, and $V(S)$. This dominance makes $V(T_1)$ [$V(T_2)$] highly correlated (anticorrelated) with $V(S)$, even though correlations between $V$ and $T_1$ ($T_2$) and between $V$ and $S$ are low (see Table A1). The anticorrelation between $V(T_2)$ and $V(S)$ results from the fact that $T_2$ and $S$, which modulate the variations of $V(T_2)$ and $V(S)$, have opposite signs. This could happen in polar regions.

TABLE A1. Correlations (Cor) between time series and products of time series shown in Fig. A1.

| | $(V, T_1)$ $(V, T_2)$ | $(V, S)$ | $(T_1, S)$ $(T_2, S)$ | $[V(T_1), V(S)]$ | $[V(T_2), V(S)]$ |
|---|---|---|---|---|---|
| Cor | 0.035 | 0.2 | −0.27 | 0.99 | −0.83 |

## REFERENCES

Beckmann, A., C. Böning, B. Brügge, and D. Stammer, 1994: On the generation and role of eddy variability in the central North Atlantic Ocean. *J. Geophys. Res.,* **99** (C10), 20 381–20 391.

Beena, B., and J.-S. von Storch, 2009: Effects of fluctuating daily surface fluxes on the time-mean oceanic circulation. *Climate Dyn.,* **33,** 1–18.

Berloff, P., 2005: Random-forcing model of the mesoscale oceanic eddies. *J. Fluid Mech.,* **529,** 71–95.

——, W. Dewar, S. Kravtsov, and J. McWilliams, 2007: Ocean eddy dyanmics in a coupled ocean–atmosphere model. *J. Phys. Oceanogr.,* **37,** 1103–1121.

Blaker, A., J. Hirschi, B. Sinha, B. Cuevas, S. Alderson, A. Coward, and G. Madec, 2012: Large near-inertial oscillations of the Atlantic meridional overturning circulation. *Ocean Modell.,* **42,** 50–56.

Eden, C., and R. Greatbatch, 2008: Towards a mesoscale eddy closure. *Ocean Modell.,* **20,** 233–239.

Fraedrich, K., 2005: Stochastic-dynamic analyses of subscale processes: Observations in the tropics and applications. *GCM ECMWF Workshop on Representation of Sub-Grid Processes Using Stochastic-Dynamic Models,* ECMWF, 65–78. [Available online at http://www.mi.uni-hamburg.de/fileadmin/files/forschung/theomet/docs/pdf/frae_ecmwf05.pdf.]

Frankignoul, C., and K. Hasselmann, 1977: Stochastic climate models. Part II: Application to sea-surface temperature anomalies and thermocline variability. *Tellus,* **29,** 289–305.

Gent, P., J. Willebrand, T. McDougall, and J. McWilliams, 1995: Parameterizing eddy-induced tracer transports in ocean circulation models. *J. Phys. Oceanogr.,* **25,** 463–474.

Gibson, J., P. Kallberg, S. Uppala, A. Hernandez, A. Nomura, and E. Serrano, 1997: ERA description. ECMWF Re-Analysis Project Rep. Series 1, 72 pp.

Hasselmann, K., 1976: Stochastic climate models, Part I. Theory. *Tellus,* **6,** 473–485.

Hoskins, B., I. James, and G. White, 1983: The shape, propagation and mean-flow interaction of large-scale weather systems. *J. Atmos. Sci.,* **40,** 1595–1612.

Jayne, S., and J. Marotzke, 2002: The oceanic eddy heat transport. *J. Phys. Oceanogr.,* **32,** 3328–3345.

Jungclaus, J., and Coauthors, 2006: Ocean circulation and tropical variability in the coupled model ECHAM5/MPI-OM. *J. Climate,* **19,** 3952–3972.

Kalnay, E., and Coauthors, 1996: The NCEP/NCAR 40-Year Reanalysis Project. *Bull. Amer. Meteor. Soc.,* **77,** 437–470.

Komori, N., W. Ohfuchi, B. Taguchi, H. Sasaki, and P. Klein, 2008: Deep ocean inertia–gravity waves simulated in a high-resolution global coupled atmosphere–ocean GCM. *Geophys. Res. Lett.,* **35,** L04610, doi:10.1029/2007GL032807.

Lemke, P., 1977: Stochastic climate models. Part 3: Application to zonally averaged energy models. *Tellus,* **29,** 385–392.

Levitus, S., and Coauthors, 1998: *Introduction*. Vol. 1, *World Ocean Database 1998,* NOAA Atlas NESDIS 18, 346 pp.

Lin, J., and J. Neelin, 2000: Influence of a stochastic moist convective parameterization on tropical climate variability. *Geophys. Res. Lett.,* **27,** 3691–3694.

Maltrud, M. E., and J. McLean, 2005: An eddy resolving global 1/10° ocean simulation. *Ocean Modell.,* **8,** 31–54.

Masumoto, Y., and Coauthors, 2004: A fifty-year eddy-resolving simulation of the world ocean–preliminary outcomes of OFES (OGCM for the earth simulator). *J. Earth Simul.,* **1,** 35–56.

McClean, J., P.-M. Poulain, J. Pelton, and M. Maltrud, 2002: Eulerian and Lagrangian statistics from surface drifters and a high-resolution pop simulation in the North Atlantic. *J. Phys. Oceanogr.,* **32,** 2472–2491.

Meijers, A., N. Bindoff, and J. Roberts, 2007: On the total, mean, and eddy heat and freshwater transports in the Southern Hemisphere of a 1/8° × 1/8° global ocean model. *J. Phys. Oceanogr.,* **37,** 277–295.

Núñez-Riboni, I., O. Boebel, M. Ollitrault, Y. You, P. Richardson, and R. Davis, 2005: Lagrangian circulation of Antarctic intermediate water in the subtropical south atlantic. *Deep-Sea Res. II,* **52,** 545–564.

Palmer, T., 2001: A nonlinear dynamical perspective on model error: A proposal for non-local stochastic-dynamic parametrization in weather and climate prediction models. *Quart. J. Roy. Meteor. Soc.,* **127,** 279–304.

Roemmich, D., and J. Gilson, 2001: Eddy transport of heat and thermocline waters in the north pacific: A key to interannual/decadal variability? *J. Phys. Oceanogr.,* **31,** 675–687.

Röke, F., 2001: An atlas of surface fluxes based on the ECMWF Re-Analysis—A climatological dataset to force global ocean general circulation models. MPI-Rep. 323, 31 pp.

Seiffert, R., and J.-S. von Storch, 2008: Impact of atmospheric small-scale fluctuations on climate sensitivity. *Geophys. Res. Lett.,* **35,** L10704, doi:10.1029/2008GL033483.

——, and ——, 2010: A stochastic analysis of the impact of small-scale fluctuations on tropospheric temperature response to $CO_2$ doubling. *J. Climate,* **23,** 2307–2319.

——, R. Blender, and K. Fraedrich, 2006: Subscale forcing in a global atmospheric circulation model and stochastic parameterisation. *Quart. J. Roy. Meteor. Soc.,* **128,** 1–17.

Smith, R., M. Maltrud, F. Bryan, and M. Hecht, 2000: Numerical simulation of the North Atlantic Ocean at 1/10°. *J. Phys. Oceanogr.,* **30,** 1532–1561.

Stammer, D., 1997: Global characteristics of ocean variability from regional TOPEX/Poseidon altimeter measurements. *J. Phys. Oceanogr.,* **27,** 1743–1769.

——, 1998: On eddy characteristics, eddy transports and mean flow properties. *J. Phys. Oceanogr.,* **28,** 727–739.

——, C. Boening, and C. Dieterich, 2001: The role of variable wind forcing in generating eddy energy in the North Atlantic. *Prog. Oceanogr.,* **48,** 289–311.

Traon, P. L., F. Nadal, and N. Ducet, 1998: An improved mapping method of multisatellite altimeter data. *J. Atmos. Oceanic Technol.,* **15,** 522–534.

Trenberth, K., 1991: Storm tracks in the Southern Hemisphere. *J. Atmos. Sci.,* **48,** 2159–2178.

von Storch, J.-S., 2004: On statistical dissipation in GCM-climate. *Climate Dyn.,* **23,** 1–15.

——, C. Eden, I. Fast, H. Haak, D. Hernandez-Deckers, E. Maier-Reimer, J. Marotzke, and D. Stammer, 2012a: An estimate of Lorenz energy cycle for the world ocean based on the 1/10° STORM/NCEP simulation. *J. Phys. Oceanogr.,* **42,** 2185–2205.

Watermann, S., and S. Jayne, 2012: Eddy-driven recirculations from a localized transient forcing. *J. Phys. Oceanogr.,* **42,** 430–447.

Wunsch, C., 1999: Where do ocean eddy heat fluxes matter? *J. Geophys. Res.,* **104,** 13 235–13 249.

Zhai, X., R. J. Greatbatch, and J.-D. Kohlmann, 2008: On the seasonal variability of eddy kinetic energy in the Gulf Stream region. *Geophys. Res. Lett.,* **35,** L24609, doi:10.1029/2008GL036412.